The Kinetics of β-Hematin Crystallization Measured by Depolarized Light Scattering

Omar Rifaie-Graham, Xiao Hua, Nico Bruns, and Sandor Balog*

Adolphe Merkle Institute, University of Fribourg Chemin des Verdiers 4, 1700 Fribourg, Switzerland

*Corresponding Author; Email: sandor.balog@unifr.ch

Malaria is caused by *Plasmodium sp.* parasites transmitted by infected female *Anopheles sp.* mosquitoes. The survival of the parasites in the host relies on detoxifying free heme by biocrystallization into insoluble crystals called hemozoin. This mechanism of self-preservation is targeted by a certain class of antimalarial drugs, which are screened and selected based on their capacity to inhibit the formation of hemozoin crystals. Therefore, experimental techniques capable of characterizing accurately the kinetics of crystal formation are valuable. Relying on the optical anisotropy of hemozoin, we describe the kinetics of β-hematin crystal formation through the statistical analysis of photon counts of dynamic depolarized light scattering (DDLS), in the absence and presence of an antimalarial drug (chloroquine, CQ). We find that CQ has an impact on both the nucleation and growth of the crystals.

Malaria is a deadly infective disease[1] of the blood that is caused by *Plasmodium sp.* parasites, which are transmitted from person to person by infected female *Anopheles sp.* mosquitoes. Inside red blood cells, the parasite degrades and digests hemoglobin to supply its own metabolism.[2,3] During this process, the parasite releases a non-digested molecule: heme. Heme is highly toxic to the parasite and disrupts the function of its cell membrane, which would

result in cell lysis and ultimately self-digestion.[4] To prevent this, the parasite neutralizes heme by biocrystallization: the oxidation and dimerization of heme is followed by a well-defined self-assembly through hydrogen bonding and π-stacking into a triclinic crystal structure (Figure 1).[5]

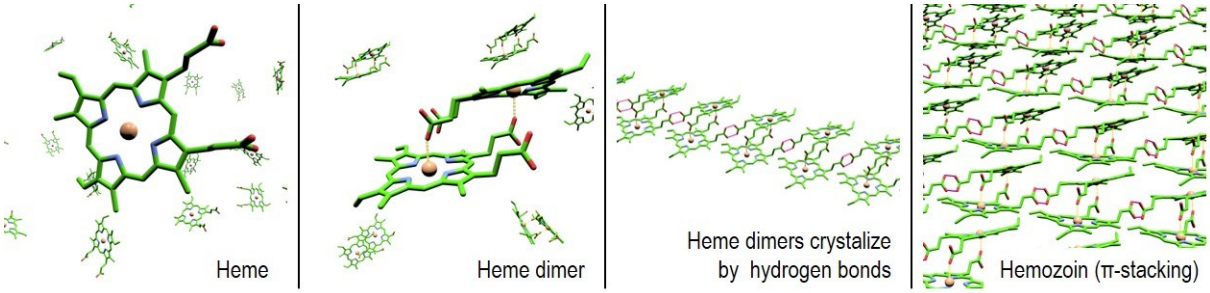

Figure 1. The envisaged route of biocrystallization of heme through dimerization and self-assembly into hemozoin. The heme molecule has a planar structure, and produces centrosymmetric μ-propionate dimers to generate the basic unit of hemozoin crystals. Then, hemozoin is formed by reciprocal hydrogen bonds between carboxylic acid groups, forming a supramolecular system that self-assembles by regular π-stacking.

Given that hemozoin crystallization is an elementary mechanism in the detoxification of heme, a key concept defining the quinoline-sp. antimalarial drugs is the inhibition of hematin self-assembly. While this approach has an acknowledged history in antimalarial chemotherapy, drug resistance has reemerged and has become responsible for the increase in malaria-related mortality, in particular in Africa.[6,7] Drug discovery necessitates high-throughput assays[8] of new compounds and a profound understanding of the mechanism and kinetics of crystallization and its inhibition.[5,9,10] The availability of synthetic hemozoin—β-hematin, whose physical properties, including structural optical and magnetic properties, are identical to hemozoin isolated from the parasite[11]—has accelerated the investigations.[12] Here we show that dynamic depolarized light scattering (also known as depolarized dynamic light scattering, DDLS) presents an outstanding potential in addressing hemozoin crystallization. The applicability of

DDLS is granted by the self-assembly of heme and hemozoin, that is, self-assembly is strictly orientation-specific and ensures that anisotropy is a long-range feature being several orders of magnitude beyond the size of the molecule. The hemozoin crystals present an elongated needle or brick-like (parallelepiped) morphology, which means, that the optical refractive index, and thus, polarizability is different along the directions defined by π-stacking and hydrogen bonding, respectively. Accordingly, the elements of the polarizability tensor are not identical. Due to this anisotropy in the polarizability, the polarization vector of the scattered light is not equal to the polarization vector of the laser light illuminating the hemozoin crystal, and the scattered light contains a 'depolarized' component (vh) perpendicular to the original polarization (vv) of the laser. Therefore, upon translational and rotational diffusion, the amplitude of depolarized scattering will fluctuate, and the rate and amplitude of the fluctuation of the scattering intensity will carry information about Brownian dynamics and particle size. It has been shown before that the statistical analysis of the photon count distribution of the scattered light describes accurately Brownian dynamics.[13,14] Therefore, we used this technique to follow the self-assembly and growth of β-hematin crystals in the absence and presence of CQ. The distribution of photon counts (n) of depolarized dynamic light scattering is[15]

(1) $$P(n) = \binom{n+M-1}{M-1} \cdot \left(\frac{M}{\langle n \rangle + M}\right)^{M} \cdot \left(\frac{\langle n \rangle}{\langle n \rangle + M}\right)^{n}.$$

$\langle n \rangle$ is linearly proportional to the mean intensity of depolarized scattering (I_{vh}) and M is a function of the Brownian dynamics of the particle (Γ) and the time interval used to count the photons (τ):

(2) $$M(\Gamma, \tau) = \frac{2 \cdot (\Gamma \cdot \tau)^2}{e^{-2 \cdot \Gamma \cdot \tau} + 2 \cdot \Gamma \cdot \tau - 1}.$$

The Brownian dynamics of the particle is described by its rotational (D_R) and translational (D_T) diffusivity[16]

(3) $$\Gamma = 6 \cdot D_R + q^2 \cdot D_T$$

where $q = 4\pi/\lambda\, n_s\, sin(\theta/2)$ is the momentum transfer, with θ being the scattering angle, λ the wavelength of the scattered waves and n_s the refractive index of the solution.[16] Using the concept of hydrodynamic radius—defined as the radius of a sphere with an equivalent diffusivity—we can determine the hydrodynamic radius of the β-hematin crystal

(4) $$D_R = \frac{k_B T}{8\,\pi\,\eta} \frac{1}{R^3}$$

(5) $$D_T = \frac{k_B T}{6\,\pi\,\eta} \frac{1}{R}$$

where R is the hydrodynamic radius, k_B the Boltzmann constant, T the temperature, η the viscosity of the solution. Starting from Equation 1, it can be shown that there is a fundamental relationship between M, the variance and mean of the photon count distribution:

(6) $$\langle n^2 \rangle - \langle n \rangle^2 = \langle n \rangle + \frac{\langle n \rangle^2}{M}$$

where

(7) $$\langle n^f \rangle \equiv \sum_{n=0}^{\infty} n^f \cdot P(n).$$

The essence of Equation 1-7 is that the mean and variance of the photon count distribution of the fluctuations of the depolarized component of the scattered light describes quantitatively Brownian dynamics, and therefore, based on the optical anisotropy of β-hematin, the mean and variance of $P(n)$ is expected to be dependent on q^2. To test this, we recorded depolarized scattering of a dilute suspension of β-hematin, and analyzed $P(n)$ at several angles (15°, 20°…45°, Experimental Section). We used a laser wavelength of $\lambda = 660$ nm, where light absorption of hemozoin and β-hematin is low (Figure 2a). Figure 2b shows the traces of photon counts recorded at a sampling rate of 19 Hz at the different angles. Both the mean and the amplitude of the fluctuations decreases with the angle of scattering. Figure 2c shows the corresponding photon count distributions, and Figure 2d shows the relaxation rate Γ—

determined at each angle via Equation 1 and 7—which exhibits a linear dependence on q^2. Therefore, β-hematin—and thus hemozoin—is indeed suitable for DDLS analysis.

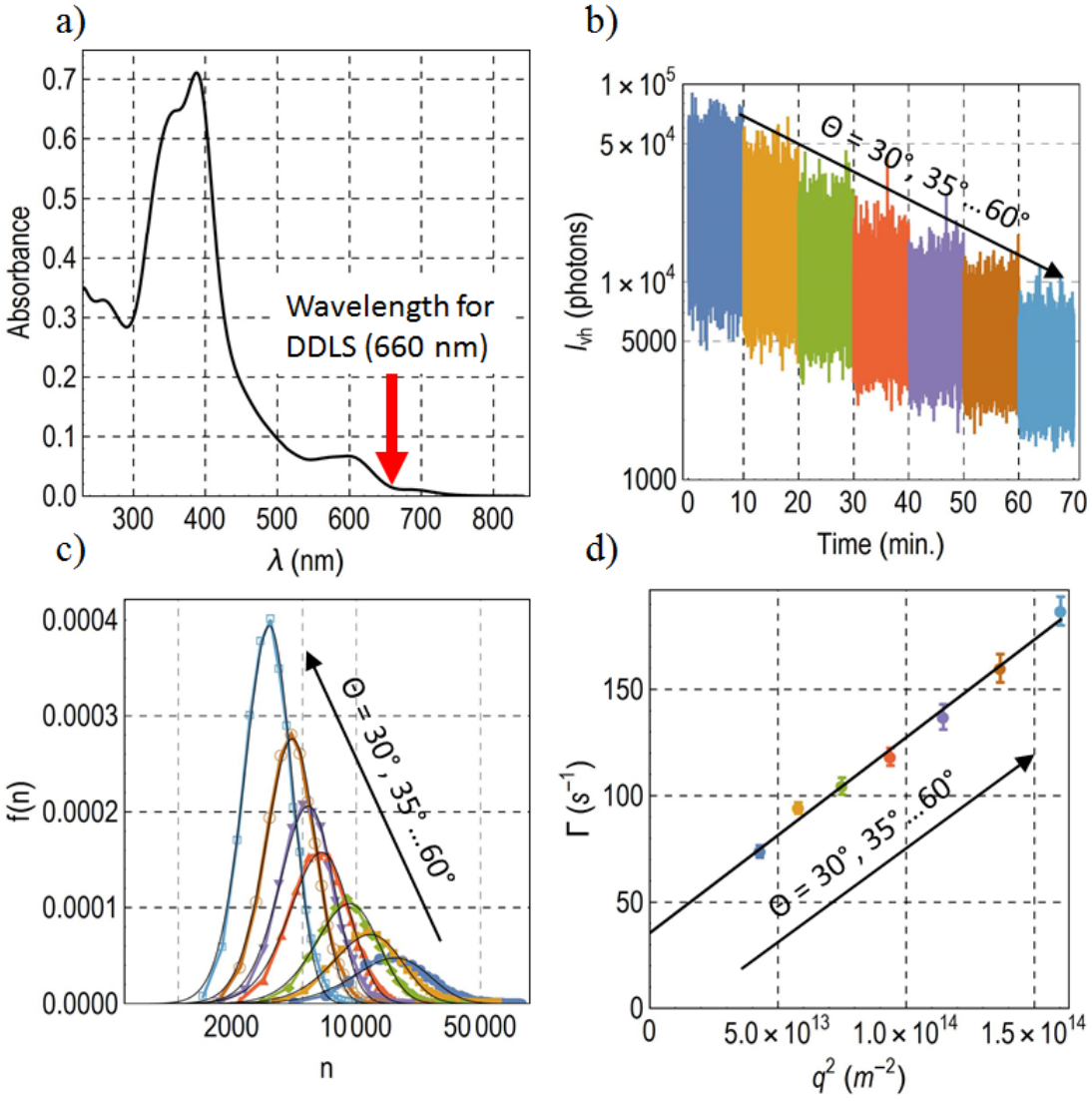

Figure 2. a) UV-Vis optical extinction spectrum of β-hematin suspended in water. To collect DDLS data, we used a laser wavelength of $\lambda = 660$ nm, where light absorption is low. b) Stream of photon counts recorded consecutively at different scattering angles. c) The corresponding photon count distributions. d) The q^2-dependence of the Brownian dynamics of the β-hematin crystals, determined from the photon counts. The data points define a straight line with a nonzero intercept. The solid line is the best linear fit that determines a hydrodynamic radius of $R_H = 309 \pm 10$ nm (estimate $\pm$ standard error).

To follow the self-assembly depicted in Figure 1, β-hematin was dissolved in sodium h ydroxide, and the addition of acetic acid triggered the isothermal recrystallization (Experimental Section). In the first experiment, the self-assembly and recrystallization of β-hematin was triggered alone, and in the second experiment, the recrystallization of β-hematin was triggered in the presence of CQ. TEM images—taken by isolating the β-hematin after 30 minutes of recrystallization time—supported by Fourier-transform infrared spectroscopy (FT-IR) and X-ray diffraction (XRD) show that self-assembly indeed resulted in crystallization (Figure 3), and consequently, depolarization is the outcome of light scattering from reassembled β-hematin. Figure 4 displays the primary steps of obtaining the necessary information from the photon counts to describe the formation of β-hematin crystals. Figure 4a shows the two 30-minutes-long traces of photon counts recorded at a sampling rate of 19 Hz. A 30-second-long period of the second trace—divided into three 10-second-long parts—is shown in Figure 4b. The corresponding photon count distributions and first two raw moments of $P(n)$ are shown in Figure 4c and d, respectively. The full length of the photon count traces were analyzed via Equation 1-7 in terms of mean scattering intensity ($I_{vh} = \langle n \rangle$) and relaxation rate ($\Gamma$). Figure 5a and b shows that I_{vh} increases and Γ decreases with crystallization time. The crystallization of β-hematin in the presence of CQ is initially rapid but considerably slows down after 3-4 minutes, and after 20 minutes, the crystallization practically levels off. The crystallization kinetics of β-hematin in the absence of CQ displays a quite different kinetic: the initial rate of crystallization is moderate but the crystals form and grow steadily.

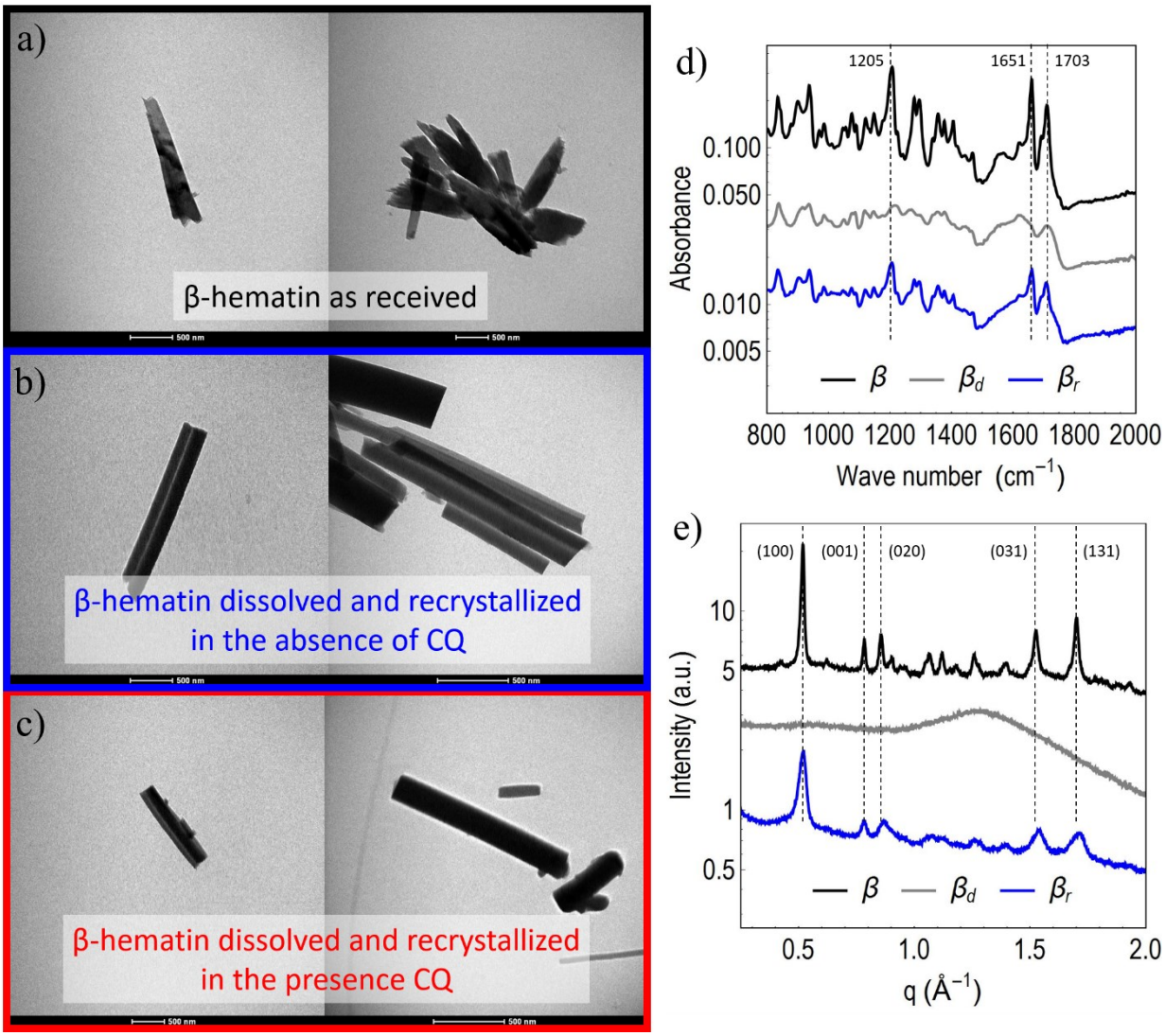

Figure 3. a)-c) Two TEM micrographs of each β-hematin sample. The scale-bars mark 500 nm. d) FT-IR absorbance spectra. β-hematin crystals as received (β, black), in dissolved non-crystalline state (β_d, gray) and recrystallized in the absence of CQ (β_r, blue). The spectra are shifted vertically for the sake of clarity. Three maxima are attributed to the chemical bonds characteristic to β-hematin: the maxima at 1205 cm^{-1} and 1651 cm^{-1} correspond to the coordinated carboxylate C—O and C=O stretches, respectively, and the maximum at 1703 cm^{-1} corresponds to the C=O stretch of the free carboxylic acid group.[10,17,18] Apart from the non-crystalline heme, these maxima are clearly visible in the FT-IR patterns. e) XRD patterns of β-hematin crystals as received (β, black), in dissolved non-crystalline state (β_d, gray) and recrystallized in the absence of CQ (β_r, blue). The Miller indices describing the orientation of

parallel crystal planes characteristic to β-hematin are indicated.[19] The absence of Bragg peaks and corresponding crystal planes in the case of non-crystalline heme is evident.

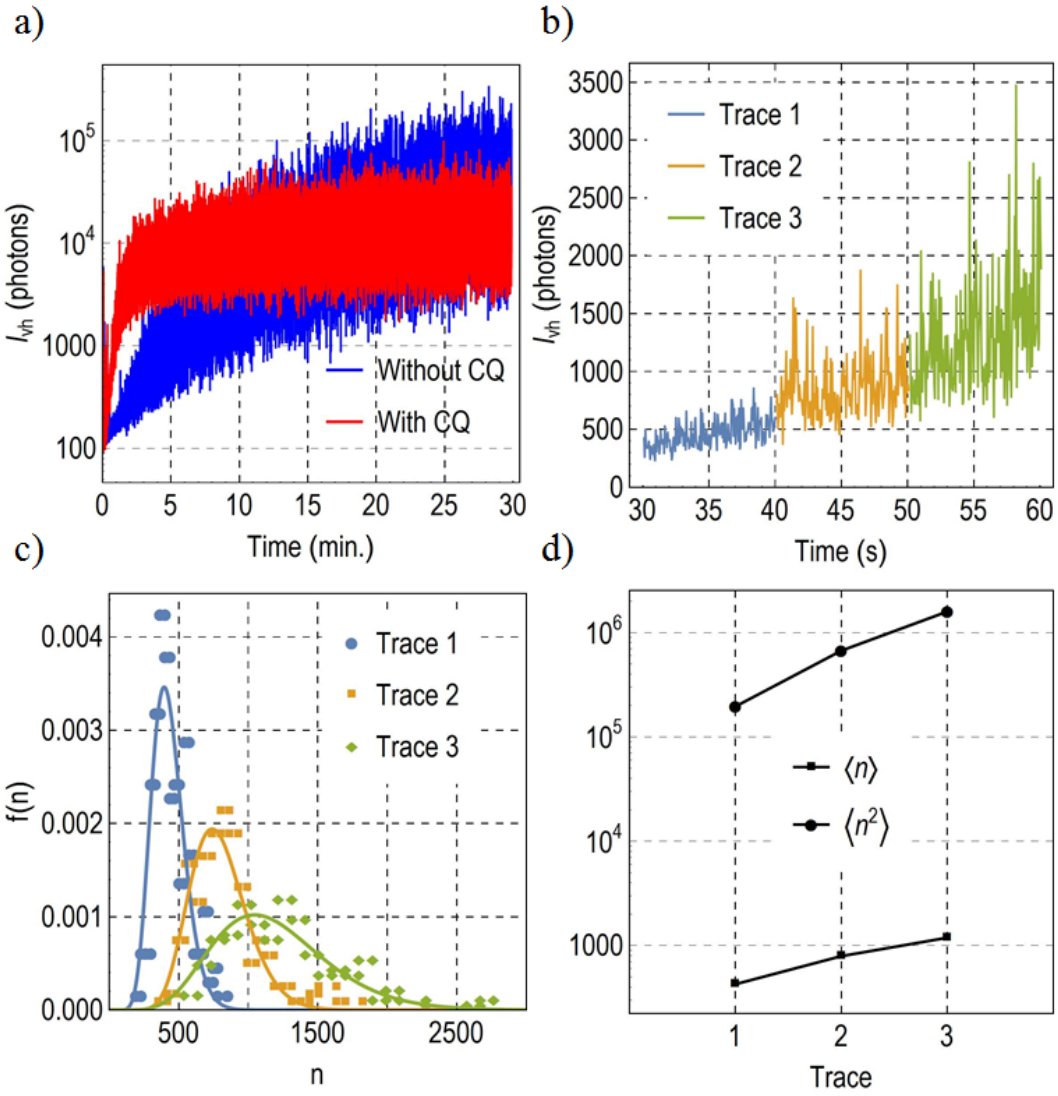

Figure 4. a) The traces of photon counts recorded during recrystallization of β-hematin in the presence of chloroquine (With CQ) and absence of chloroquine (Without CQ). b) A 30-second-long period of the photon count trace in the presence of chloroquine divided into three equal parts. c) The corresponding photon count distributions, and d) their first two raw moments.

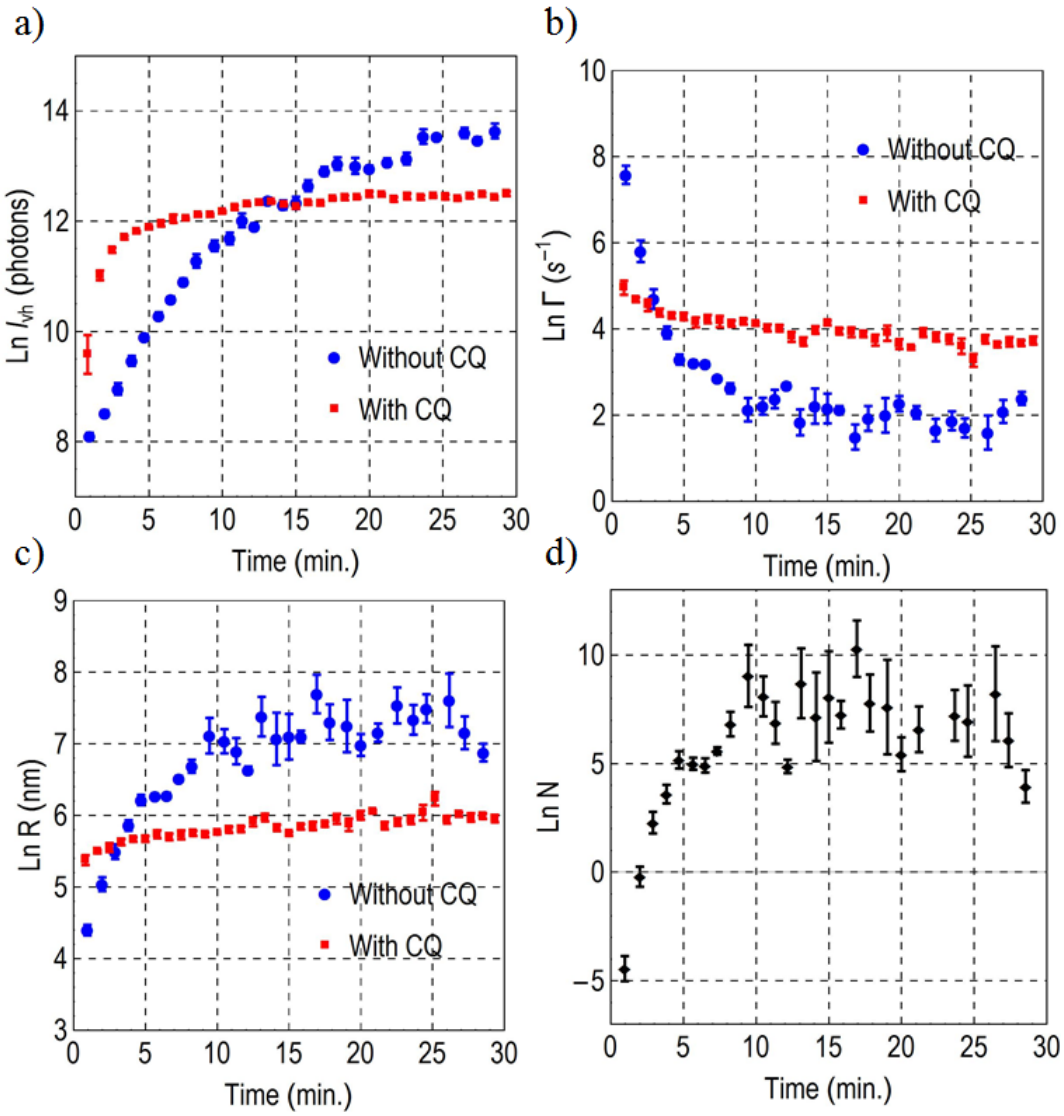

Figure 5. The crystallization kinetics of β-hematin in the presence of chloroquine (With CQ) and absence of chloroquine (Without CQ). a) The natural logarithm of the mean scattering intensity as a function of crystallization time. b) The natural logarithm of the relaxation rate as a function of crystallization time. c) The natural logarithm of the hydrodynamic radius as a function of crystallization time. d) The natural logarithm of the relative number of β-hematin crystals: $N = C_{with\ CQ}/C_{wo\ CQ}$, where C denotes the concentration of the crystal nuclei formed in the absence and presence of CQ. For the sake of clarity, the data points on each panel present the average of five measurements, and the error bars present the standard errors.

To understand the meaning of these observations, we adopt the approximation of the Rayleigh-Ganz-Debye (RGD) theory.[20] The mean intensity may be expressed as $I_{vh} \propto C \cdot V^2$, where C is the concentration and V is the volume of the β-hematin crystals. The volume of the particle is proportional to the hydrodynamic volume, which may be expressed by the hydrodynamic radius (R, Figure 5c) as $V = 4/3\,\pi \cdot R^3$, where R is determined from Γ (Equation 3). The formation of the crystals results from nucleation and growth. First, small clusters form and lose and gain molecules until a specific critical size is reached (called: nucleus or seed), from where growth occurs. V is proportional to the degree of growth, and the concentration of β-hematin (C) is proportional to the concentration of the nuclei. Accordingly, the concentration of crystals may be expressed as $C \propto I_{vh}/R^6$. Thus, we estimate the ratio of the concentrations of β-hematin crystals grown in the presence of CQ and in the absence of CQ as $N = C_{with\ CQ}/C_{wo\ CQ}$. Figure 5c and d show that in the presence of CQ the number of nuclei is higher, but the crystals do not reach the same volume as in the absence of CQ.

The latter is in complete agreement with the earlier picture that the drug-heme complex negatively affects crystal formation.[21] One the one hand, there is a well-supported and evidence-based consensus that the growth of β-hematin crystals follow a classical mechanism, in which the deposition of solute heme builds and spreads new crystal layers.[22,23] The deposition is monomolecular and follows a first-order chemical kinetics. In this classical process, a new layer is deposited onto the smooth surface of the previous layer, and its height is typically one lattice spacing.[24] The decreased rate of crystal growth in the presence of CQ is attributed to the adsorption and relatively strong binding of CQ to the facets of the crystal, which may arrest the classical buildup and spread of new crystal layers.[10,25,26] Our results indeed show that—as expected—crystal growth is hindered by the presence of CQ (Figure 5c). In the presence of CQ, the eventual hydrodynamic radius (close to 400 nm) is less than fourth

of the size measured in the absence of CQ (more than 1800 nm), where the crystals may grow as large as convenient in the given experimental environment.

On the other hand, crystal growth and crystal birth (nucleation) are independent and concurrent processes, and therefore, there is an alternative hypothesis that explains the inhibition of crystallization by the formation of CQ-heme complexes.[27-29] This route of inhibition reduces the concentration of heme, and thus, directly affects the nucleation rate as well.[10] We observed in our system that more crystals—however, considerably smaller—are formed in the presence of CQ and grew faster (Figure 5c and d). This shows that CQ did not reduce the nucleation rate. To account for this evidence, we offer the following argument: nucleation requires a considerably smaller amount of molecules than the additional growth of an already existing crystal whose surface is increasing with volume. Therefore, if nucleation is not affected but crystal growth is hindered by the presence of CQ, the rate of nucleation will increase owing to the availability of the heme that is eventually not able to attach to the surface of the crystals. In the absence of CQ, the growth of a crystal is uninhibited, and thus, it can keep growing, which requires increasing heme equivalents, hence the rate of nucleation will decrease achieving a plateau in DDLS.

To summarize, we believe that dynamic light scattering, DDLS in particular, could easily find its way to antimalarial studies addressing biocrystallization. We showed that DDLS is a straightforward assay in the context of quinoline-sp. antimalarial chemotherapy, where the inhibition of heme self-assembly and crystal growth is the primary target. While the parameters of hemozoin biocrystallization we studied here may be specific and not the only possible choice, the analysis is based on general physical and mathematical principles underlying the theory of light scattering. These principles ensure that the technique is suitable for any system exhibiting the physical features of self-assembly, completely independently of the parameters of the system, such as chemical reactions and concentrations. Additionally, the approach is

suitable[30,31] for miniaturization and integration into microfluidic platforms and lab-on-a-chip assays,[32] where automation and parallelization for high-throughput is desired.[13] Furthermore, unlike other techniques,[33] depolarized light scattering enables a cost-effective design,[13] and fiber-optics based detection probes small volumes on the order of nanoliters.[34]

Experimental Section

Synthetic hemozoin (β-hematin) was purchased from InvivoGen (San Diego, CA) and was used as received. Sodium hydroxide (≥ 98%), chloroquine diphosphate salt (≥98%) (CQ), and acetic acid (≥ 99.7%) were purchased from Sigma Aldrich. β-hematin was suspended in ultrapure water. Ultrapure water was obtained from a Purelab Flex II (Veolia water system) with a resistance of 18.2 mΩ, and an LC208 purification pack. The ultrapure water was filtered with a Nylon 66 syringe filter with a pore size of 0.22 μm (BGB Analytik, Switzerland). 0.10 mg (0.15 mmol) of β-hematin were weighed in a glass vial and were suspended in 3 mL of the filtered water. To a standard cell culture glass tube, 3 mL of the filtered water were introduced, and 200 μL of the β-hematin suspension were added yielding a suspension with a concentration of 2.22 μg mL^{-1} (3.44 nmol mL^{-1}). The suspension was sonicated for three minutes in a sonicator bath (Sonoswiss SW3) to yield a homogeneous suspension of non-aggregated crystals. The crystallization of β-hematin was achieved by employing a described procedure.[35] Briefly, a stock solution of β-hematin was prepared by dissolving 0.10 mg (0.15 μmol) β-hematin in 1 mL of 0.4 M sodium hydroxide. The latter was diluted ten times in 0.4 M sodium hydroxide to generate a second stock solution. Individually, 0.7 mL of each stock solution was aliquoted into two different cell culture glass tubes. To each test tube, 0.62 mL of ultrapure water was added. The recrystallization of β-hematin was initiated by the addition of 0.68 mL of acetic acid. The final pH of the solution was 2.9. To observe the influence of CQ in the crystallization kinetics, the same procedure as for the crystallization of isolated heme was employed, but pure acetic

acid was substituted by a solution of 20.60 mg mL^{-1} (64.41 μmol mL^{-1}) of CQ. The final CQ concentration in the crystallization reactions was 0.66 mg mL^{-1} (2.08 μmol mL^{-1}).

The UV-Vis measurement was performed on an Analytik Jena Specord 50 Plus spectrophotometer, using a disposable semi-micro poly(methyl methacrylate) cuvette (path length: 1 cm).

Transmission electron microscopy (TEM) images were obtained using a FEI Tecnai Spirit at 120 kV. The images were recorded at a resolution of 2048x2048 pixels (Veleta CCD camera, Olympus). In the case of the imaging of hemozoin yielded from the crystallization reactions, the same conditions as in the DDLS experiments were employed. Then, the reaction volume was filtered with a syringe filter, and the filtrate was extensively washed with ultrapure water. Then, the crystals were retrieved by smearing the filter with 1 mL of ultrapure water. 5 μl of the β-hematin suspensions were drop-casted onto a carbon-film square mesh copper grid (Electron Microscopy Sciences, CF-300-Cu) and the solvent was allowed to dry overnight.

Fourier-transform infrared spectroscopy (FT-IR) spectra were collected by using a Perkin Elmer 65 spectrometer in attenuated total reflection (ATR) mode.

X-ray diffraction (XRD) data was collected using a STOE STADI P diffractometer with a step size of 0.2 °(2θ) in transmission mode and a Cu target (λ = 1.5414 Å). The detector channels were calibrated by a Si standard. The *x*-axis is converted into *q*-space by the equation $q = 4\pi/\lambda\, sin(\theta)$, where 2θ is the angle between the axes of the X-ray beam and detector, respectively, and λ the wavelength of the diffracted X-ray waves.

To obtain a sufficient signal-to-noise ratio for the FT-IR and XRD experiments, 5 mg of hemozoin were dissolved in 1.32 mL of a 0.4 M NaOH aqueous solution, to which 1.24 mL of ultrapure water were added. The solution was stirred with a magnetic stirring bar. The crystallization process was initiated by the addition of 1.4 mL of acetic acid and the mixture was allowed to stir for a period of 2 h. The resulting crystals were isolated from the solution by

vacuum filtration over a polyvinylidene fluoride membrane filter (Duapore, pore size 0.45 μm). Then, the filtrate was washed thoroughly with dimethyl sulfoxide (DMSO) to remove non-crystalized hematin. Finally, the filtrate was washed with ultrapure water to eliminate any remaining NaOH. Finally, the filtrate was then dried in a vacuum oven at 65 °C overnight. To isolate non-crystalline hematin, 5 mg of hemozoin were dissolved in 1.32 mL of 0.4 M NaOH aqueous solution. To eliminate the NaOH salts, the solution was passed through a silica gel plug with methanol as the mobile phase. Finally, the solvent was removed by rotary evaporation.

Light scattering data were collected at constant temperature (21 °C) using a commercial goniometer instrument (3D LS Spectrometer, LS Instruments AG, Switzerland). The primary beam was formed by a linearly polarized and collimated laser beam (Cobolt 05-01 diode pumped solid state laser, λ = 660 nm, $P_{max.}$ = 500 mW), and the scattered light was collected by single-mode optical fibers equipped with integrated collimation optics. With respect to the primary beam, depolarized scattering was observed via cross-polarizers. The incoming laser beam passed through a Glan-Thompson polarizer with an extinction ratio of 10^{-6}, and another Glan-Thompson polarizer, with an extinction ratio of 10^{-8}, was mounted in front of the collection optics. The collected light was coupled into an avalanche photo diode detector (Perkin Elmer, Single Photon Counting Module) via laser-line filters. The photon counts were obtained at a sampling rate of 19 Hz. Each sample was ~0.05 s long, which also defined the lower limit of the available integration times.

Acknowledgement

The authors thank the Swiss National Science Foundation for the financial support through the National Center of Competence in Research (NCCR) Bio-Inspired Materials and the project PP00P2_172927. SB is also grateful for the financial support of the Adolphe Merkle Foundation and the University of Fribourg.

Conflict of Interest

The authors declare no conflict of interest.

Keywords

antimalarial drugs, crystallization, depolarized light scattering, dynamic light scattering, hemozoin, β-hematin, photon counting

References

[1] Murray, C. J. L.; Rosenfeld, L. C.; Lim, S. S.; Andrews, K. G.; Foreman, K. J.; Haring, D.; Fullman, N.; Naghavi, M.; Lozano, R.; Lopez, A. D., *Lancet* **2012**, 379, 413.

[2] Sullivan, D. J.; Matsumura, S.; Steinbüchel, A., Hemozoin: a Biocrystal Synthesized during the Degradation of Hemoglobin. In *Biopolymers Online*, 2005.

[3] Coronado, L. M.; Nadovich, C. T.; Spadafora, C., *Biochim. Biophys. Acta, Gen. Subj.* **2014**, 1840, 2032.

[4] Sigala, P. A.; Goldberg, D. E., *Annu. Rev. Microbiol.* **2014**, 68, 259.

[5] Weissbuch, I.; Leiserowitz, L., *Chem. Rev.* **2008**, 108, 4899.

[6] Klein, E. Y., *Int. J. Antimicrob. Agents* **2013**, 41, 311.

[7] White, N. J., *J. Clin. Invest.* **2004**, 113, 1084.

[8] Sinha, S.; Sarma, P.; Sehgal, R.; Medhi, B., *Front. Pharmacol.* **2017**, 8.

[9] Fidock, D. A.; Rosenthal, P. J.; Croft, S. L.; Brun, R.; Nwaka, S., *Nat. Rev. Drug Discovery* **2004**, 3, 509.

[10] Gildenhuys, J.; Roex, T. l.; Egan, T. J.; de Villiers, K. A., *J. Am. Chem. Soc.* **2013**, 135, 1037.

[11] Pagola, S.; Stephens, P. W.; Bohle, D. S.; Kosar, A. D.; Madsen, S. K., *Nature* **2000**, 404, 307.

[12] Pandey, A. V.; Singh, N.; Tekwani, B. L.; Puri, S. K.; Chauhan, V. S., *J. Pharm. Biomed. Anal.* **1999**, 20, 203.

[13] Bossert, D.; Natterodt, J.; Urban, D. A.; Weder, C.; Petri-Fink, A.; Balog, S., *J. Phys. Chem. B* **2017**, 121, 7999.

[14] Bossert, D.; Crippa, F.; Petri-Fink, A.; Balog, S., *Anal. Chem.* **2018**, 90, 3656.

[15] Goodman, J. W., *Statistical Optics*. Wiley: **2000**.

[16] Pecora, R., *Dynamic Light Scattering: Applications of Photon Correlation Spectroscopy*. Plenum Press: New York, **1985**.

[17] Slater, A. F.; Swiggard, W. J.; Orton, B. R.; Flitter, W. D.; Goldberg, D. E.; Cerami, A.; Henderson, G. B., *Proc. Natl. Acad. Sci.* **1991**, 88, 325.

[18] Chen, M. M.; Shi, L.; Sullivan, D. J., *Mol. Biochem. Parasitol.* **2001**, 113, 1.

[19] Solomonov, I.; Osipova, M.; Feldman, Y.; Baehtz, C.; Kjaer, K.; Robinson, I. K.; Webster, G. T.; McNaughton, D.; Wood, B. R.; Weissbuch, I.; Leiserowitz, L., *J. Am. Chem. Soc.* **2007**, 129, 2615.

[20] Barber, P. W.; Wang, D.-S., *Appl. Opt.* **1979**, 18, 962.

[21] Sullivan, D. J.; Gluzman, I. Y.; Russell, D. G.; Goldberg, D. E., *Proc. Natl. Acad. Sci.* **1996**, 93, 11865.

[22] Olafson, K. N.; Ketchum, M. A.; Rimer, J. D.; Vekilov, P. G., *Proceedings of the National Academy of Sciences* **2015**, 112, 4946.

[23] Olafson, K. N.; Ketchum, M. A.; Rimer, J. D.; Vekilov, P. G., *Crystal Growth & Design* **2015**, 15, 5535.

[24] Vekilov, P. G., *Crystal Growth & Design* **2007**, 7, 2796.

[25] Buller, R.; Peterson, M. L.; Almarsson, Ö.; Leiserowitz, L., *Crystal Growth & Design* **2002**, 2, 553.

[26] Fitzroy, S.-M.; Gildenhuys, J.; Olivier, T.; Tshililo, N. O.; Kuter, D.; de Villiers, K. A., ***Convert Citations and BibliographyConvert Citations and Bibliography****Langmuir* **2017**, 33, 7529.

[27] Cohen, S. N.; Phifer, K. O.; Yielding, K. L., *Nature* **1964**, 202, 805.

[28] Chou, A. C.; Chevli, R.; Fitch, C. D., *Biochemistry* **1980**, 19, 1543.

[29] Egan, T. J., *Journal of Inorganic Biochemistry* **2006**, 100, 916.

[30] Destremaut, F.; Salmon, J.-B.; Qi, L.; Chapel, J.-P., *Lab. Chip* **2009**, 9, 3289.

[31] Chastek, T. Q.; Beers, K. L.; Amis, E. J., *Rev. Sci. Instrum.* **2007**, 78, 072201.

[32] Kolluri, N.; Klapperich, C. M.; Cabodi, M., *Lab. Chip* **2018**, 18, 75.

[33] Sandlin, R. D.; Fong, K. Y.; Wicht, K. J.; Carrell, H. M.; Egan, T. J.; Wright, D. W., *Int. J. Parasitol. Drugs. Drug. Resist.* **2014**, 4, 316.

[34] Gisler, T.; Rüger, H.; Egelhaaf, S. U.; Tschumi, J.; Schurtenberger, P.; Rička, J., *Appl. Opt.* **1995**, 34, 3546.

[35] Blauer, G.; Akkawi, M., *Biochemical Journal* **2000**, 346, 249.